

Reaction Mechanisms of $C_2Cl_3 + NO_2$ via Nitro and Nitrite Adducts

Kunhui Liu, Tiancheng Xiang, Weiqiang Wu, Shaolei Zhao, and Hongmei Su*

State Key Laboratory of Molecular Reaction Dynamics, Beijing National Laboratory for Molecular Sciences (BNLMS), Institute of Chemistry, Chinese Academy of Sciences Beijing 100080, China

Received: April 10, 2008; Revised Manuscript Received: August 12, 2008

The atmospherically and environmentally important reaction of chlorinated vinyl radical with nitrogen dioxide ($C_2Cl_3 + NO_2$) is investigated by step-scan time-resolved Fourier transform infrared emission spectroscopy and electronic structure calculations. Vibrationally excited products of CO, NO, Cl_2CO , and NO_2 are observed in the IR emission spectra. Geometries of the major intermediates and transition states along the potential energy surface are optimized at the B3LYP/6-311G(d) level, and their energies are refined at the CCSD(T)/6-311+G(d) level. The reaction mechanisms are characterized to be barrierless addition–elimination via nitro ($C_2Cl_3-NO_2$) and nitrite (C_2Cl_3-ONO) adducts. Four energetically accessible reaction routes are revealed, i.e., the decomposition of the nitrite adduct forming $C_2Cl_3O + NO$ and its sequential dissociation to $CO + NO + CCl_3$, the elimination of ClNO from the nitrite adduct leading to $ClNO + Cl_2CCO$, the Cl-atom shift of the nitrite adduct followed by the decomposition to $CCl_3CO + NO$, and the O-atom shift of the nitro adduct followed by C–C bond cleavage forming $ClCNO + Cl_2CO$. In competition with these reactive fluxes, the back-decomposition of nitro or nitrite adducts leads to the prompt formation of vibrationally excited NO_2 and the long-lived reaction adducts facilitate the vibrational energy transfer. Moreover, the product channels and mechanisms of the $C_2Cl_3 + NO_2$ reaction are compared with the $C_2H_3 + NO_2$ reaction to explore the effect of chlorine substitution. It is found that the two reactions mainly differ in the initial addition preferentially by the N-attack forming nitro adducts (only N-attack is plausible for the $C_2H_3 + NO_2$ reaction) or the O-attack forming nitrite adducts (O-attack is slightly more favorable and N-attack is also plausible for the $C_2Cl_3 + NO_2$ reaction). The addition selectivity can be fundamentally correlated to the variation of the charge density of the end carbon atom of the double bond induced by chlorine substitution due to the electron-withdrawing effect of chlorine groups.

1. Introduction

Reactions involving transient species of ONOX (X = OH, F, Cl) are of significant importance for global atmospheric chemistry and thus have been constantly studied.^{1–6} For example, for the three-body association reaction of $Cl + NO_2$, it has been shown both experimentally⁷ and theoretically^{3,8} that both ClONO (nitrite adduct) and ClNO₂ (nitro adduct) are yielded and the former nitrite adduct accounts for the yield dominantly by about 80%. The termolecular rate constant has been determined to be $7.2 \times 10^{-31} \text{ cm}^6 \text{ molecule}^{-2} \text{ s}^{-1}$.⁹ The reversed $ClO + NO$ is an exothermic bimolecular reaction characterized mainly by the dissociation of the adduct ClONO to the products of $Cl + NO_2$, and the reaction rate constant is $1.6 \times 10^{-11} \text{ cm}^3 \text{ molecule}^{-1} \text{ s}^{-1}$.³

In comparison, for hydrocarbon radicals reacting with NO_2 which should have more complicated mechanism, such as the C_2H_3 radical reaction with NO_2 , investigations are relatively scarce. The C_2H_3 radical is very reactive toward NO_2 , and the reaction occurs via bimolecular processes. Geppert et al.¹⁰ measured the rate constant for this reaction to be $[(4.19 \pm 0.05) \times 10^{-11}](T/300 \text{ K})^{-0.60 \pm 0.07} \text{ cm}^3 \text{ molecule}^{-1} \text{ s}^{-1}$ and observed NO as the only product. They also performed calculations at the level of RMP2/6-311+G(d,p) and revealed that the reaction proceeds through the intermediates of nitroethylene ($C_2H_3NO_2$) and vinyl nitrite (C_2H_3ONO). The N-site attack of NO_2 was found to be favored, and thus the nitroethylene is initially formed. The energized nitroethylene can surmount the barrier

rearranging to vinyl nitrite which subsequently decomposes into the final products of $C_2H_3O + NO$. The nitro–nitrite rearrangements are found to be crucial in the mechanism. The following possible reaction pathways were proposed.

	ΔH (kJ·mol ⁻¹) (from the ab initio calculation, ref 10)
$C_2H_3 + NO_2 \rightarrow C_2H_3O + NO$	–206.3
$\rightarrow CH_3CO + NO$	–269.8
$\rightarrow C_2H_2 + HNO_2$	–203.8

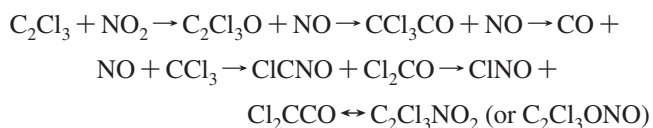
It would be interesting to study the title reaction $C_2Cl_3 + NO_2$ which might feature both characters of the $Cl + NO_2$ and $C_2H_3 + NO_2$ reactions and thus is expected to have rich and complicated chemical transformations. Moreover, valuable insights can be gained to the influence of chlorine substitution on the reaction mechanisms by comparing the $C_2Cl_3 + NO_2$ reaction with the $C_2H_3 + NO_2$ reaction.

C_2Cl_3 radicals are known to be involved in the most important and sensitive reactions affecting the burning and pyrolysis of chlorine-rich unsaturated chlorinated hydrocarbons (CHCs), especially during incineration of municipal solid waste (MSW) such as poly(vinyl chloride),^{11–14} which generally releases bad pollutants to atmosphere. It is therefore of fundamental importance to study the $C_2Cl_3 + NO_2$ reaction for developing a better understanding of the combustion chemistry of CHCs and related atmospheric chlorine chemistry.

* Corresponding author. E-mail: hongmei@iccas.ac.cn.

Except for a few kinetics measurements on the reaction rate constants for the reaction of C_2Cl_3 with either O_2 or Cl_2 ,^{15,16} the elementary reaction products, channels, and mechanisms for the C_2Cl_3 reactions are generally unknown. Systematic studies to characterize the elementary reactions of the C_2Cl_3 radicals are in progress in our laboratory. As a serial work prior to this study, we have studied the reaction of C_2Cl_3 radical with O_2 both theoretically¹⁷ and experimentally.¹⁸ For the title reaction $C_2Cl_3 + NO_2$, there is no data available for the reaction rate constant. The only reported study is our very preliminary experiments¹⁹ with only the identification of Cl_2CO , NO , and CO as the reaction products. The detection of the products was incomplete because the detector used, $InSb$, can only record IR spectral bands higher than 1850 cm^{-1} , and thus molecules with IR-active bands at lower vibrational frequencies were missed.

In this work, we intend to study the $C_2Cl_3 + NO_2$ reaction comprehensively by combining the experimental measurements with the electronic structure calculations. The elementary reaction products are detected by means of step-scan time-resolved Fourier transform infrared emission (TR-FTIR) spectroscopy which is an effective technique probing multiple IR-active reaction products in real time due to its multiplex advantage and nanosecond time resolution. Two detectors, $InSb$ and MCT , are used together to obtain full scope spectra and complete identification of the IR-active reaction products. Electronic structure calculations at the $CCSD(T)/6-311+G(d)//B3LYP/6-311G(d)$ level are performed to characterize the reaction mechanisms forming these products. By exploring the energies and geometries of the major intermediates and transition states along the potential energy surface, the minimum energy reaction paths for the energetically accessible product channels are obtained. In combination with the experimental TR-FTIR spectroscopic detection of the reaction products, the following reaction channels and their formation mechanisms are revealed for the first time, viz.:



Moreover, the product channels and mechanisms of the $C_2Cl_3 + NO_2$ reaction are compared with those of the $C_2H_3 + NO_2$ reaction to explore the influence of chlorine substitution. The influence is correlated to the variation of the charge density of the double-bond carbon atom induced by chlorine substitution due to the electron-withdrawing effect of chlorine groups.

2. Experimental and Theoretical Methods

The reaction products are monitored by step-scan, TR-FTIR spectroscopy.^{18,20} The instrument comprises a Nicolet Nexus 870 step-scan FTIR spectrometer, Lambda Physik (Compex-Pro102) excimer laser, and a pulse generator (Stanford Research DG535) to initiate the laser pulse and achieve synchronization of the laser with data collection, two digitizers (internal 100 kHz 16-bit digitizer and external 100 MHz 14-bit GAGE 8012A digitizer) which offer fast time resolution and a wide dynamic range as needed, and a personal computer to control the whole experiment. The detector used in this experiment is the liquid nitrogen cooled $InSb$ detector or $MCT-A$ detector.

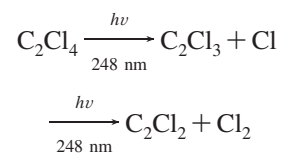
The reaction is initiated in a stainless steel flow reaction chamber. A pair of parallel multilayer coated mirrors (reflectivity $R > 0.95$ at 248 nm) reflect the UV laser beam multiple times to increase the photolysis zone. C_2Cl_3 radicals are generated by 248 nm photodissociation ($50\text{ mJ}\cdot\text{cm}^{-2}\cdot\text{pulse}^{-1}$, 10 Hz

repetition rate) of C_2Cl_4 . Samples of C_2Cl_4 ($\geq 99\%$) and NO_2 ($\geq 99.5\%$) enter the flow chamber 1 cm above the photolysis beam via needle valves. The chamber is pumped by an $8\text{ L}\cdot\text{s}^{-1}$ mechanical pump, and the stagnation pressure of the chamber is measured by an MKS capacitance monometer. The constant pressure of sample is maintained by adjusting the pumping speed and the needle valves. Typically, C_2Cl_4 (10 Pa) and NO_2 (70 Pa) are used to keep pseudo-first-order reaction conditions. Transient infrared emission is collected by a pair of gold-coated Welsh cell spherical mirrors and collimated by a CaF_2 lens to the step-scan Fourier spectrometer (Nicolet Nexus 870). The flow rate is fast enough to replenish the sample at each laser pulse running normally at a repetition rate of 10 Hz as described in detail previously.¹⁸

Theoretically, the geometries of the reactants, products, various intermediates, and transition states are optimized using the hybrid density functional theory, i.e., Becke's three-parameter nonlocal exchange functional with the nonlocal correlation functional of Lee, Yang, Parr (B3LYP) with the standard 6-311G(d) basis sets.^{21,22} For the current reaction involving eight heavy atoms, the B3LYP/6-311G(d) level of theory is a balanced method considering the computational efficiency and accuracy. Moreover, the B3LYP/6-311G(d) level of theory is able to suppress effectively the problem of spin contaminant. Harmonic vibrational frequencies and the zero-point energies (ZPE) are calculated at the same level with the optimized geometries. The intermediates are characterized by all the real frequencies. The transition states are confirmed by only one imaginary frequency. Connections of the transition states between two local minima have been confirmed by intrinsic reaction coordinate (IRC) calculations at the B3LYP/6-311G(d) level.²³ To obtain more reliable energetic data, single-point electronic energies are calculated at the $CCSD(T)/6-311+G(d)$ level using the B3LYP/6-311G(d) optimized geometries. All of the theoretical calculations are performed with the Gaussian 03 program package.²⁴

3. Results and Discussion

3.1. Experimental Detection of the Reaction Products. In the present experiment, C_2Cl_3 radicals were generated by KrF laser photolysis of C_2Cl_4 at 248 nm and are the only reactive radicals produced from the photolysis:¹⁵



The Cl atoms do not react with NO_2 via bimolecular processes to produce $ClO + NO$ since the reaction is endothermic by $42.4\text{ kJ}\cdot\text{mol}^{-1}$.³ Instead, the reaction of Cl atoms with NO_2 occurs via three-body association with a termolecular rate constant of $7.2 \times 10^{-31}\text{ cm}^6\text{ molecule}^{-2}\text{ s}^{-1}$.⁹ Under the present total pressure of 80 Pa, it is estimated that the three-body association reaction occurs slowly on a time scale of tens of milliseconds. The other photofragments, the chlorinated acetylene C_2Cl_2 and Cl_2 , are stable molecules. They are not expected to react with NO_2 molecules as fast as the radical fragment C_2Cl_3 (the reaction rate constant of C_2Cl_3 radical with NO_2 was not measured before, but it should be comparable to its analogy $C_2H_3 + NO_2$ reaction with the room-temperature reaction rate constant reported¹⁰ to be $(4.19 \pm 0.05) \times 10^{-11}\text{ cm}^3\text{ molecule}^{-1}\text{ s}^{-1}$). Therefore, all the coexisted photofragments Cl , Cl_2 , and C_2Cl_2 are not likely to compete with the highly reactive C_2Cl_3 radicals

in their reaction with NO_2 molecules within the time scale of experimental measurements, i.e., tens of microseconds.²⁵ The photodissociation of C_2Cl_4 molecules provide a good source of C_2Cl_3 radicals for the study of its consecutive reaction with NO_2 molecules.

It is first desirable to characterize the energy of the reactant, i.e., the photolytically produced C_2Cl_3 radicals. UV absorption spectra measured by Berry²⁶ shows that chloroethylenes C_2H_3Cl , $C_2H_2Cl_2$, C_2HCl_3 , and C_2Cl_4 all have two absorption bands in a region between 260 and 140 nm. A broad absorption band at ~ 200 nm is assigned to the $\pi^* \leftarrow \pi$ transition. Both 193 and 248 nm excitation falls into this absorption band, corresponding to the $\pi^* \leftarrow \pi$ transition. Except C_2Cl_4 , the photodissociation of a series of chloroethylenes including C_2H_3Cl , $C_2H_2Cl_2$, and C_2HCl_3 has been well studied with photofragment ion imaging or photofragment translation spectroscopy.^{27–32} These studies have demonstrated that following the $\pi^* \leftarrow \pi$ transition at 193 nm, the photodissociation mechanisms for various chloroethylenes are basically the same and the dominant pathway is the C–Cl bond rupture through predissociation via the crossing of the $\pi\pi^*$ state with the repulsive $\pi\sigma^*$ state to give rise to fast Cl atoms. The measured average translational energy fraction ranges from 43.4%, 42.2%, and 36.6% for C_2H_3Cl , $C_2H_2Cl_2$, and C_2HCl_3 photodissociation, respectively. The photodissociation of C_2Cl_4 should follow the same mechanism to other chloroethylenes, and thus the translational energy release can be evaluated to be mostly close to that of C_2HCl_3 , maybe a little smaller according to the trend shown with the Cl-substitution. Supposing 36% of energy released into the translation, the average translational energy and internal energy of the C_2Cl_3 radicals is estimated to be 11.6 and 61.7 $\text{kJ}\cdot\text{mol}^{-1}$, respectively, with the available energy of 97.4 $\text{kJ}\cdot\text{mol}^{-1}$ from the photodissociation of C_2Cl_4 at 248 nm. The photolytically produced C_2Cl_3 radicals are vibrationally excited. The vibrational relaxation could possibly occur on a time scale of at least a few microseconds for the C_2Cl_3 radical. Thus, hot C_2Cl_3 radicals are involved in the consecutive reaction with NO_2 molecules. But no IR emission signal due to vibrationally excited C_2Cl_3 radicals was detected in the TR-FTIR spectra in the reference experiment of the 248 nm photolysis of pure C_2Cl_4 . The reason is that the only vibrational mode of C_2Cl_4 falling within the spectral detection range, the C=C stretch of 1634 cm^{-1} , has very weak IR intensity. This provides a background-free detection of the reaction of C_2Cl_3 with NO_2 .

Due to the small absorption cross section of NO_2 molecules at 248 nm ($3.8 \times 10^{-20} \text{ cm}^2$), the possible interference caused by the photodissociation of NO_2 ($NO_2 \rightarrow O + NO$) can be suppressed effectively by adjusting the laser power intensity. It is estimated that only a negligible amount (approximately 0.2%) of NO_2 molecules undergoes dissociation at the laser power of 50 $\text{mJ}\cdot\text{cm}^{-2}$, and as a result, no IR emission signals due to the photofragment NO was observed in the reference experiment when pure NO_2 was irradiated at 248 nm.

Once the gaseous mixture of 70 Pa NO_2 and 10 Pa C_2Cl_4 was irradiated at 248 nm, several IR emission bands were observed as shown in Figure 1. These IR emission bands are originated from the vibrationally excited products of the $C_2Cl_3 + NO_2$ reaction. Laser power dependence of the product yields has been measured to be 1.2 ± 0.2 , indicating that the photolysis is a one-photon process and only the subsequent $C_2Cl_3 + NO_2$ reaction gives rise to these product IR emission signals.

IR emission spectra record the infrared fluorescence emitted from vibrationally excited species due to a set of vibrational transitions $\nu \rightarrow \nu - 1$, and thus the band is generally much

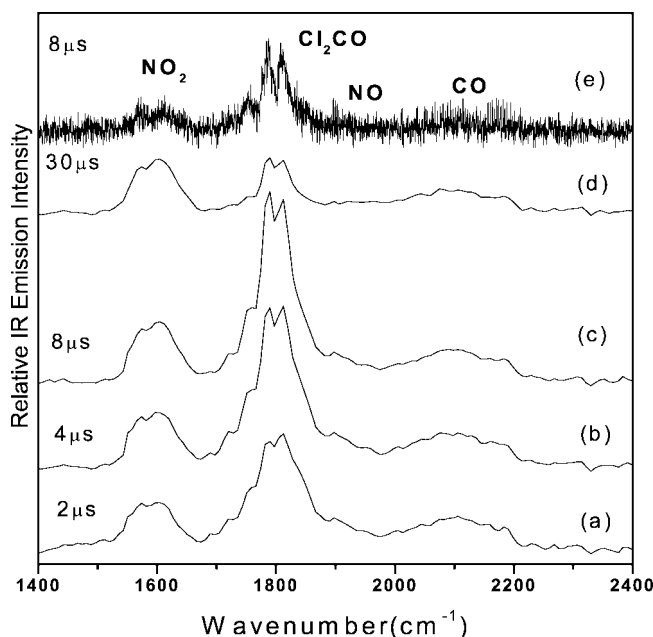


Figure 1. Product TR-FTIR emission spectra from the reaction of $C_2Cl_3 + NO_2$ taken at typical delay times from 2 to 30 μs after initiation of the reaction by 248 nm laser photolysis. The spectra were collected using the lower sensitivity, but higher spectral range (720–5000 cm^{-1}), MCT-A detector: (a–d) spectral resolution of 16 cm^{-1} ; (e) spectral resolution of 0.5 cm^{-1} .

broader than normal static IR absorption spectra and the peak center exhibits somewhat red shift relative to the fundamental frequency position ($1 \rightarrow 0$). As shown in the 16 cm^{-1} resolution spectra in Figure 1, there are basically three IR emission bands spanning 1500–1700, 1700–2000, and 2000–2200 cm^{-1} , respectively. To help assigning these bands, high-resolution (0.5 cm^{-1}) spectra were collected and the typical spectra are also included in Figure 1. The rotationally resolved emission band from 2000 to 2200 cm^{-1} is ascribed to several sets of rovibrational transitions of $CO(\nu \rightarrow \nu - 1)$. The 1700–2000 cm^{-1} emission is actually comprised of two bands. The rotationally irresolvable band centered at 1802 cm^{-1} is most likely ascribed to the polyatomic molecule $Cl_2CO \nu_1$ (fundamental frequency at 1827 cm^{-1}).¹⁸ The other rotationally resolved band superimposed on top of the Cl_2CO band is due to the rovibrational transitions of $NO(\nu \rightarrow \nu - 1)$. The partially resolved band from 1500 to 1700 cm^{-1} should arise from $NO_2 \nu_3$ (fundamental frequency at 1618 cm^{-1}).

The spectra shown in Figure 1 were collected with the lower sensitivity, but wider spectral range (720–5000 cm^{-1}), MCT-A detector. The detector can record the full scope emission bands of the four products of CO, NO, Cl_2CO , and NO_2 , allowing a complete identification of the IR-active reaction products. But due to its lower sensitivity, the signal-to-noise (S/N) ratio of the high-resolution (0.5 cm^{-1}) spectra is relatively poor. To obtain 0.5 cm^{-1} spectra with better S/N, the higher sensitivity detector InSb was applied in another measurement, and the spectra are displayed in Figure 2. The two rotationally resolved emission bands of CO and NO can be explicitly observed and identified with the InSb detector. However, only part of the spectra of Cl_2CO is recorded with InSb because the probe cuts off at 1850 cm^{-1} .

A spectral fitting has been performed for the rotationally resolved CO and NO emission bands using the spectral constants of these two molecules and a nonlinear least-squares fitting program which has been described in detail elsewhere.³³

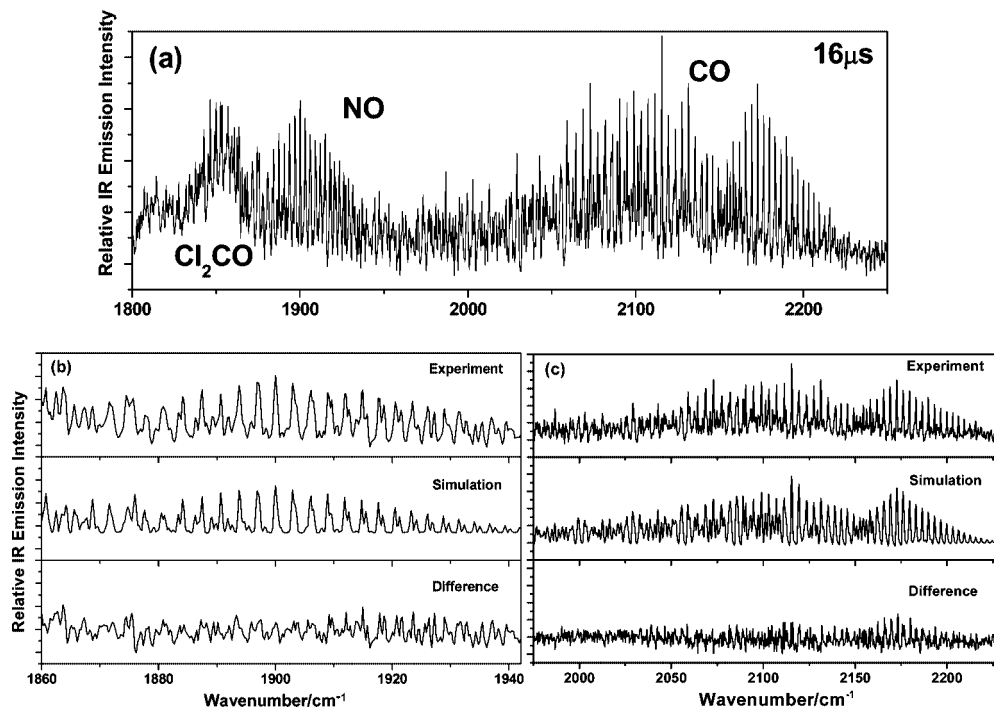
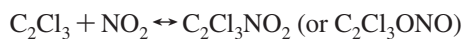


Figure 2. (a) Representative experimental TR-FTIR emission spectra at the reaction time of 16 μs collected using the higher sensitivity InSb detector which cuts off at 1850 cm^{-1} . (b and c) Representative spectral fitting results for the IR emission bands of the products NO (b) and CO (c). The difference between the experimental spectrum and the corresponding fitted spectrum is also shown at the bottom.

Representative fitting results, shown in Figure 2, demonstrate further that these two bands are ascribed to CO and NO molecules. The best fitted rotational temperature is 300 K, indicating that the rotational excitation has been thermalized. About 60 collisions take place within 16 μs at the total pressure of 80 Pa, which is sufficient to quench the rotational excitation to room temperature but not to alter the vibrational excitation much. For the 16 μs NO emission band, the best fitted vibrational populations of NO are 1/0.28/0.23 for the vibrational levels of $\nu = 1-3$ indicating that the band is comprised of three $\Delta\nu = -1$ progressions of rovibrational transitions. For the 16 μs CO emission band, the best fitted vibrational populations of CO are 1/0.33/0.17/0.14/0.09/0.07/0.06/0.04 for the vibrational levels of $\nu = 1-8$. The IR emission band of CO is therefore attributed to eight $\Delta\nu = -1$ progressions of rovibrational transitions.

All of the product signals appear within 2 μs and grow to their maximum intensity at roughly 8 μs . The identical rise time of the four emission bands indicates that the four products CO, NO, Cl_2CO , and NO_2 are originated from the same reaction, i.e., the $\text{C}_2\text{Cl}_3 + \text{NO}_2$ reaction. Same as the formation kinetics of the other three vibrationally excited products, the IR emission from NO_2 rises promptly after the laser pulse suggesting that NO_2 should be ascribed to the formation-dissociation equilibrium of the reaction adducts $\text{C}_2\text{Cl}_3\text{NO}_2$ or $\text{C}_2\text{Cl}_3\text{ONO}$.



The formation of the long-lived collision complex $\text{C}_2\text{Cl}_3\text{NO}_2$ or $\text{C}_2\text{Cl}_3\text{ONO}$ facilitates the energy transfer between C_2Cl_3 and NO_2 , leading to the prompt formation of vibrationally excited NO_2 . The hot C_2Cl_3 radicals possess enough internal energy, estimated to be 61.7 $\text{kJ}\cdot\text{mol}^{-1}$, to excite the antisymmetric stretch mode of NO_2 , and thus the IR emission band of NO_2 (ν_3) is observed as shown in Figure 1. It is not likely that the vibrationally excited NO_2 arise from the vibrational energy transfer between NO_2 and other hot molecules (reactants or

products) without forming a complex because this kind of vibrational energy transfer occurs on a slower time scale with the formation rate of NO_2 being slower than that of CO, NO, and Cl_2CO , but in fact these four species are formed with identical rates as shown in Figure 1.

3.2. Reaction Mechanisms. The products CO, NO, Cl_2CO , and NO_2 from the $\text{C}_2\text{Cl}_3 + \text{NO}_2$ reaction have been identified from the time-resolved IR emission spectral measurements. Electronic structure calculations are performed to characterize the reaction mechanisms forming these products. The reaction between the two doublet reactants can proceed either on the singlet surface or the triplet surface. The possibility of the reaction proceeding on the triplet surface has been excluded because the calculation shows that significant entrance barriers exist on the triplet surface. In addition, no triplet reaction products are observed in the experiment. Therefore, the following discussion is based on the electronic structure calculations on the singlet surface. Geometries of the reactants, products, various intermediates, and transition states are optimized at the B3LYP/6-311G(d) level, and their single-point energies are refined at the CCSD(T)/6-311+G(d) level using the B3LYP/6-311G(d) optimized geometries. Figures 3 and 4 present the optimized structures and energy diagram of the key intermediates and transition states along the potential energy surface, respectively.

Detailed reaction mechanisms are revealed for the thermodynamically accessible reaction channels listed in Table 1. As shown in Table 1, the predicted heats of reaction based on the CCSD(T)/6-311+G(d)//B3LYP/6-311G(d) level of calculation agree well with the experimental values. Thus, the present computational method is expected to provide reliable energetic and mechanistic information for the $\text{C}_2\text{Cl}_3 + \text{NO}_2$ reaction.

3.2.1. Initial Association. Figure 4 shows the profiles of the potential energy surface for the $\text{C}_2\text{Cl}_3 + \text{NO}_2$ reaction. For conciseness, only the energetically accessible reaction routes related to the formation of the observed reaction products are

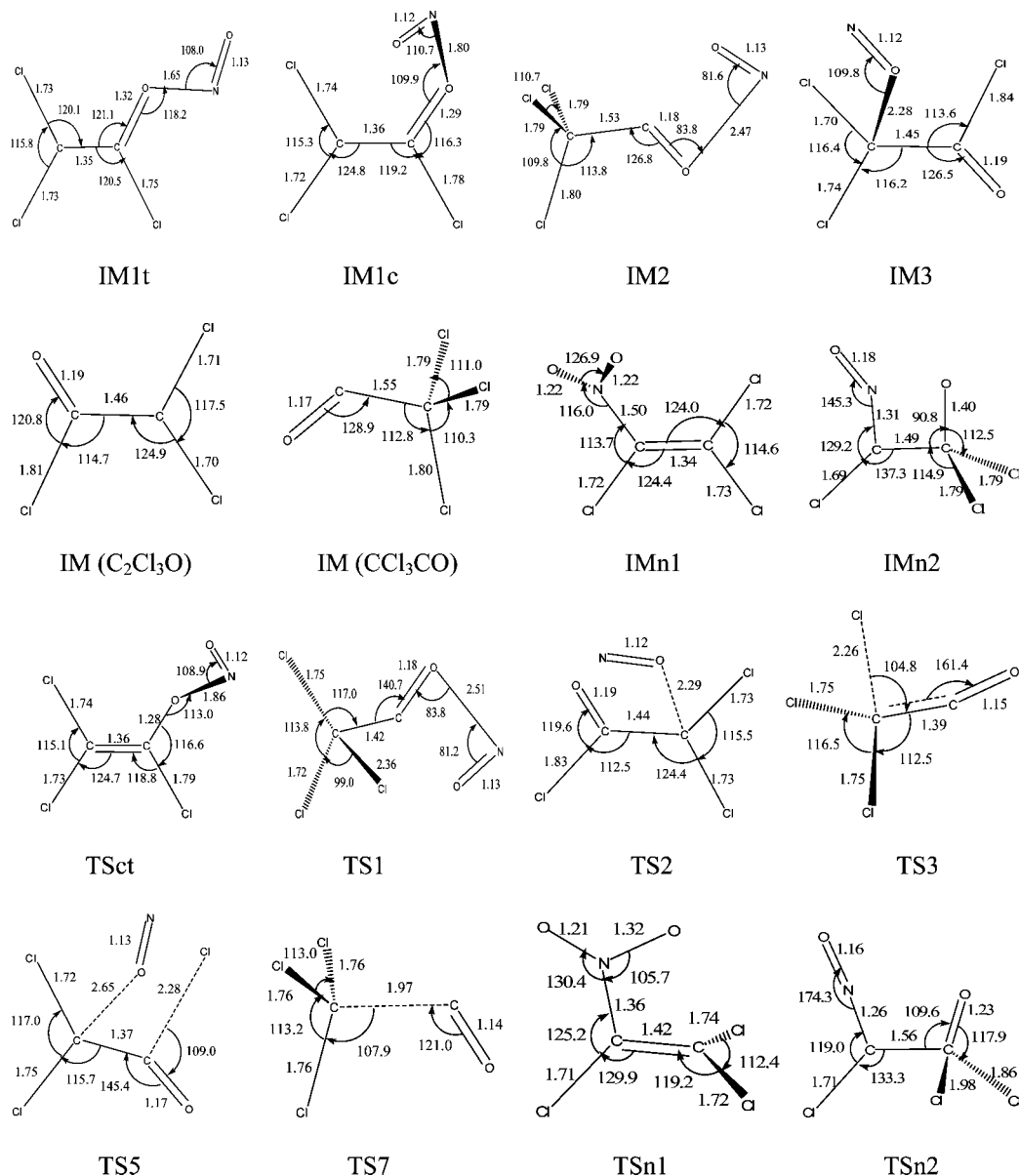


Figure 3. Structures of the intermediates and transition states involved in the $C_2Cl_3 + NO_2$ reaction. Bond distances are in angstroms, and bond angles are in degrees.

displayed. The reaction starts with the barrierless addition of the NO_2 to C_2Cl_3 radicals in two ways: the N-attack forming the nitro adduct $C_2Cl_3-NO_2$ (IMn1) and O-attack forming the nitrite adduct C_2Cl_3-ONO . The initial O-attack leads to the trans conformation nitrite adduct IM1t which isomerizes to the cis conformation nitrite adduct IM1c subsequently via a low barrier of $10.3 \text{ kJ}\cdot\text{mol}^{-1}$. But the nitro–nitrite rearrangement (IMn1 \rightarrow IM1t) requires surmounting a high barrier of $222.2 \text{ kJ}\cdot\text{mol}^{-1}$ which is irrelevant to the mechanism discussion and thus not depicted in Figure 4.

Overall, this reaction can be regarded as recombination processes between two radicals without an entrance barrier. Both the N-attack nitro adduct and O-attack nitrite adduct can be formed directly from the reactants. This can be confirmed by calculating the relaxed potential energy curves for the formative process of IMn1 and IM1t at the B3LYP/6-311G(d) level as shown in Figure 5. For the formative process of IMn1, the forming C–N bond is fixed at the values from 1.3 to 4.0 Å with an interval of 0.1 Å and from 4.0 to 10.0 Å with larger intervals, and the other geometric parameters are optimized for

each value of the C–N distance. For the formative process of IM1t, the forming C–O bond is fixed at the values from 1.2 to 4.0 Å with an interval of 0.1 Å and from 4.0 to 10.0 Å with larger intervals, and the other geometric parameters are optimized for each value of the C–O distance. In both scanning processes, the geometries still resemble their initial N-attack nitro or O-attack nitrite character without rearranging to each other. The further optimization of the two minima along the potential energy curves leads to the intermediate IMn1 with the equilibrium C–N distance of 1.50 Å and IM1t with the equilibrium C–O distance of 1.32 Å, respectively. The binding energy of IMn1 and IM1t are further refined at the CCSD(T)/6-311+G(d) level to be 235.3 and $263.8 \text{ kJ}\cdot\text{mol}^{-1}$, respectively. As clearly exhibited in Figure 5, both formative processes proceed on attractive potential energy surfaces, indicating that the N-attack nitro adduct and O-attack nitrite adduct can both be formed directly from the reactants barrierlessly. In view of the binding energy, the O-attack addition forming nitrite adducts is slightly more favorable than the N-attack addition forming

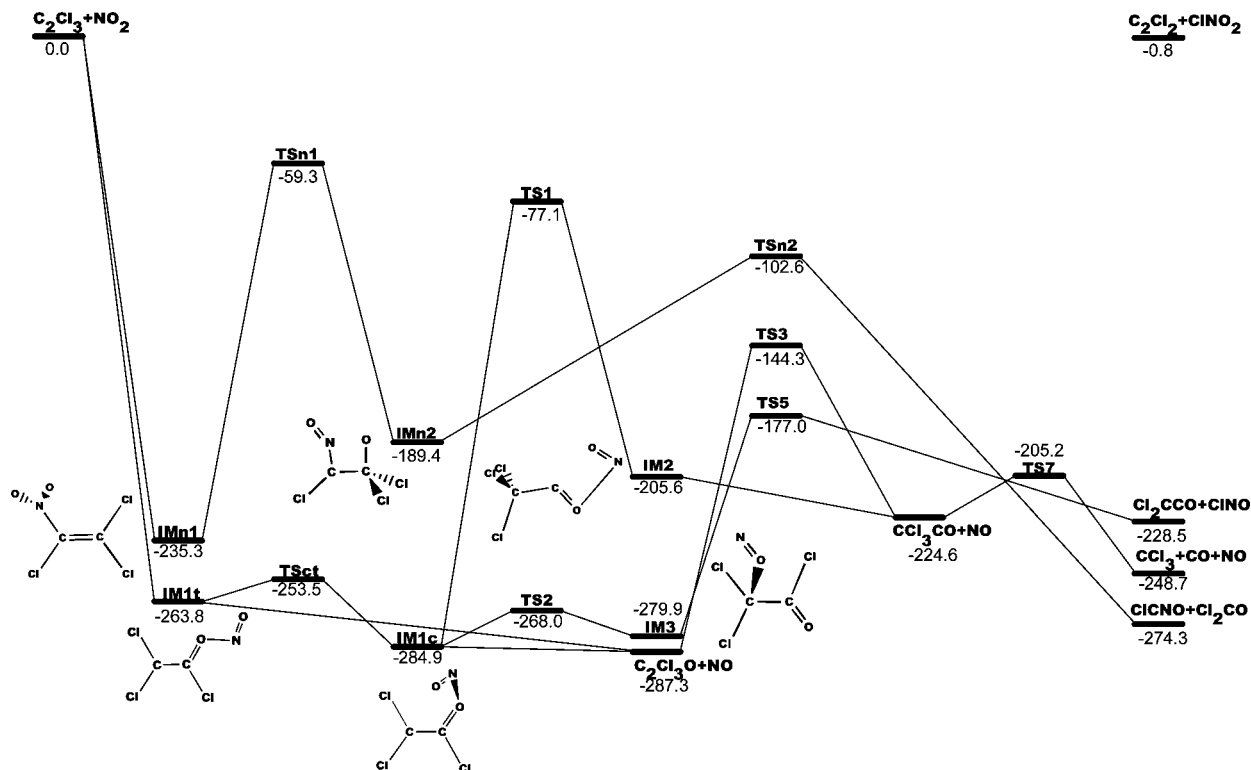


Figure 4. Profiles of the potential energy surface for the $C_2Cl_3 + NO_2$ reaction. The indicated energies (in $\text{kJ}\cdot\text{mol}^{-1}$) are obtained at the CCSD(T)/6-311+G(d)//B3LYP/6-311G(d) level of calculation. All the energies given are relative to the reactants, and structures of crucial reaction intermediates are also depicted.

TABLE 1: Predicted Heats of Reaction Based on the Electronic Structure Calculations and the Available Experimental Values

	ΔH ($\text{kJ}\cdot\text{mol}^{-1}$) (exptl) ^a	ΔH ($\text{kJ}\cdot\text{mol}^{-1}$) (CCSD(T)/ 6-311+G(d)) ^b
$C_2Cl_3 + NO_2 \rightarrow C_2Cl_3O + NO$	-285.6	-287.3
$\rightarrow CCl_3CO + NO$	-201.7	-224.6
$\rightarrow CO + NO + CCl_3$	-219.3	-248.7
$\rightarrow ClCNO + Cl_2CO$		-274.3
$\rightarrow ClNO + Cl_2CCO$		-228.5
$\rightarrow C_2Cl_2 + ClNO_2$	-3.1	-0.8
$\leftrightarrow C_2Cl_3NO_2$ (or C_2Cl_3ONO)		-235.3 (or -284.9)

^aThe experimental ΔH are obtained using the data in NIST webbook (<http://webbook.nist.gov>). ^bThe ΔH obtained from the electronic structure calculations of this work.

nitro adducts. Both adducts are highly energized and followed with isomerization or decomposition leading to final products.

3.2.2. Pathway via Nitro Adducts. Starting from the nitro adduct $C_2Cl_3-NO_2$ (IMn1), there is a four-center isomerization route leading to the intermediate IMn2 via a transition state of TSn1 with a fairly high barrier of $176.0 \text{ kJ}\cdot\text{mol}^{-1}$. With the strengthening of the C–N bond, one of the N–O bonds elongates and the leaving O atom is shifted to the C2 atom forming the intermediate IMn2. Meanwhile, the CC bond is lengthened and weakened to a single bond from double bond. Subsequently, the CC bond of IMn2 breaks readily to form the final products ClCNO + Cl_2CO via the transition state TSn2.

3.2.3. Pathway via Nitrite Adducts. In parallel to the nitro adduct $C_2Cl_3-NO_2$ (IMn1) route, the reaction can proceed through nitrite adducts C_2Cl_3-ONO . The initially formed trans C_2Cl_3-ONO IM1t isomerizes to the cis C_2Cl_3-ONO IM1c from which three reaction routes are open. The energetically most favorable route is the facile dissociation of IM1c $C_2Cl_3-O^1NO^2$

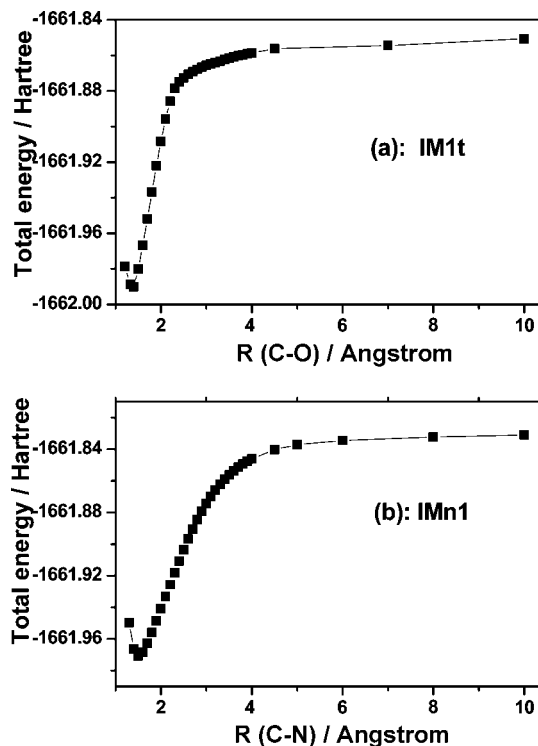


Figure 5. Relaxed potential energy curves for the formative process of the nitrite adduct IM1t (a) and the nitro adduct IMn1 (b) in the $C_2Cl_3 + NO_2$ reaction calculated at the B3LYP/6-311G(d) level. R is the bond distance.

forming $C_2Cl_3O + NO$. In the loosely structured intermediate IM1c, the O^1-N bond (1.80 \AA) is significantly longer than that (1.19 \AA) in NO_2 . Thus, the O^1-N bond has been significantly weakened when NO_2 is added to C_2Cl_3 and the O^1-N bond is

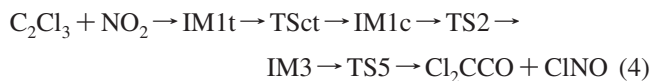
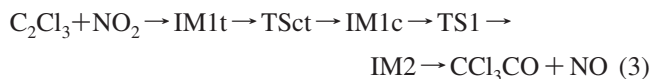
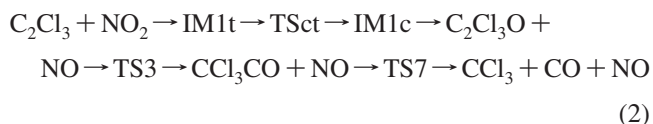
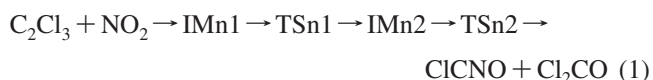
naturally cleaved afterward. The dissociation is barrierless and even slightly exoergic, yielding more energized fragments of $C_2Cl_3O + NO$. The subsequent isomerization of the C_2Cl_3O radical surmounts a barrier of $143.0 \text{ kJ}\cdot\text{mol}^{-1}$ forming CCl_3CO radical which may further dissociate to the smaller products of $CCl_3 + CO$ readily with surmounting a low barrier of $19.4 \text{ kJ}\cdot\text{mol}^{-1}$. Overall, this reaction route is characterized by the two-step dissociation of the nitrite adduct C_2Cl_3-ONO (IM1c), yielding NO and CO in sequence. It should be confident that the $C_2Cl_3O + NO$ are the nascent products of the $C_2Cl_3 + NO_2$ reaction. The subsequent isomerization and dissociation of this channel may contribute to the formation of the products of $CCl_3CO + NO$ and $CCl_3 + CO + NO$.

The second reaction route starting from IM1c involves a Cl-atom shift from C1 atom to C2 atom forming the intermediate CCl_3CONO (IM2) via a transition state TS1 which lies $77.1 \text{ kJ}\cdot\text{mol}^{-1}$ below the reactants. The subsequent dissociation of IM2 is also barrierless and thus feasible, yielding the products of $CCl_3CO + NO$ which may further dissociate to $CCl_3 + CO + NO$.

The third reaction route starts from the isomerization of IM1c $C_2Cl_3-O^1NO^2$ to the intermediate IM3 which can be described as an internal abstraction of the $N-O^2$ moiety from C1 atom to C2 atom accompanied with the breaking of the significantly weakened O^1-N bond (the bond length to be 1.80 \AA). This isomerization process requires overcoming a fairly low barrier of $16.9 \text{ kJ}\cdot\text{mol}^{-1}$ and thus is facile. Sequentially, the four-center elimination of ClNO from the intermediate IM3 gives rise to the final products of $Cl_2CCO + ClNO$.

Other reaction routes have also been explored. For example, in analogy to the $C_2H_3 + NO_2$ reaction, there should also be a channel producing $C_2Cl_2 + ClNO_2$. The calculation shows that this channel is slightly exothermic by only $0.8 \text{ kJ}\cdot\text{mol}^{-1}$ and proceeds through the elimination of ClNO₂ from the intermediate IM1c with surmounting a huge barrier which is $147.2 \text{ kJ}\cdot\text{mol}^{-1}$ above the reactants and thus is energetically inaccessible.

3.2.4. Comparison with the Experiment. In summary, there are four reaction routes via either the nitro adduct or the nitrite adduct revealed in the above discussion, namely,



All channels are exothermic, and all barriers are below the reactants and thus energetically accessible. The reaction route 2 involving the barrierless decomposition of the nitrite adduct IM1c forming $C_2Cl_3O + NO$ should be the most energetically favorable, and thus the $C_2Cl_3O + NO$ channel is predicted to be the major reaction channel. The products of NO and CO observed in the IR emission spectra are therefore mainly arising from this channel and its sequential dissociations. On the other hand, detection of the strong vibrational excitation of the products of NO up to $\nu = 3$ and CO up to $\nu = 8$ consists with the calculated large exothermicity of these channels. The

reaction route 4 proceeds through fairly low barriers and is also facile. In comparison, the reaction routes 1 and route 3 are rate-limited by surmounting a high energy barrier in the first step of the adduct isomerization and are less favorable. But owing to the large amount of excess energy deposited into the nitro and nitrite adducts, these reaction routes are all energetically accessible, and therefore corresponding products NO, CO, and Cl_2CO are observed in the IR emission spectra. Kinetically, the four reaction routes should compete with each other, and this might be the reason why neither product ClNO or Cl_2CCO via the reaction route 4 is observed in the IR emission spectra. Calculations of the reaction rate constants should help in evaluating the branching ratios for various reaction pathways, but it is beyond the scope of the current study.

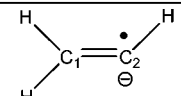
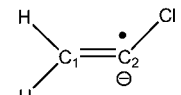
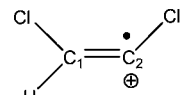
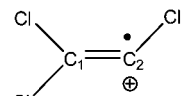
It is interesting that vibrationally excited NO_2 is observed simultaneously with the other reaction products as the back-decomposition of the nitro $C_2Cl_3NO_2$ or nitrite C_2Cl_3ONO adduct, most likely, the nitro adduct $C_2Cl_3NO_2$. As shown in Figure 4, for $C_2Cl_3NO_2$ the forward isomerization reaction proceeds via TSn1 and requires surmounting a barrier nearly as high as the back-dissociation energy of the adducts. In addition, the backward decomposition to reactants gains entropy, whereas the forward reaction via tight, lower energy transition state (TSn1) leading to products loses entropy despite its large exothermicity. Consequently, the backward decomposition of the energized adduct $C_2Cl_3NO_2$ to reactants is expected to compete with the forward reactive fluxes forming various products. Especially for the initial photolytically produced hot C_2Cl_3 radicals possessing internal energy of approximately $61.7 \text{ kJ}\cdot\text{mol}^{-1}$, the backward reaction is competitive and becoming even more favored than the forward reaction if the reactant possesses high enough energy.³⁴ As the vibrationally excited C_2Cl_3 radicals relax to the ground state by collisional energy transfer, the backward reaction shuts off and the forward reaction becomes dominant. The low-energy part of the population makes the major contribution to the forward reactive flux, whereas the high-energy part contributes to the backward decomposition.

The covalent interaction between NO_2 and C_2Cl_3 in the adducts significantly facilitates energy transfer, allowing prompt production of the vibrationally excited NO_2 . The O^1-N bond (1.80 \AA) in the nitrite C_2Cl_3ONO adduct is significantly longer than that (1.19 \AA) in the free NO_2 molecules. As a result, it is anticipated that the antisymmetric stretch of NO_2 is vibrationally excited, and this has been clearly observed in the IR emission spectra. Similar enhancement of vibrational energy transfer due to the formation of the long-lived reaction adducts has also been observed before.³⁴

3.3. Comparison with the $C_2H_3 + NO_2$ Reaction. In comparison with the $C_2H_3 + NO_2$ reaction,¹⁰ the mechanisms of the $C_2Cl_3 + NO_2$ reaction are similar and the dominant product channel is also the same, i.e., the decomposition of the nitrite adduct C_2Cl_3-ONO forming $C_2Cl_3O + NO$. However, some differences do exist indicating that the chlorination of the vinyl radical tends to influence the reaction to some extent.

In the $C_2H_3 + NO_2$ reaction,¹⁰ the reaction route to produce $C_2H_3O + NO$ was found to proceed through the rearrangement of the N-attack adduct nitroethylene $C_2H_3-NO_2$ to vinyl nitrite C_2H_3-ONO followed with subsequent decomposition. The rate-limiting step is the nitro-nitrite rearrangement surmounting a high barrier of $230.3 \text{ kJ}\cdot\text{mol}^{-1}$. In comparison, the analogous reaction route leading to $C_2Cl_3O + NO$ in the $C_2Cl_3 + NO_2$ reaction is through the decomposition of the O-attack nitrite adduct C_2Cl_3-ONO which can be formed directly from the reactants. There are no barriers along the reaction route.

TABLE 2: Mulliken Atomic Charge Calculated at B3LYP/6-311g(d,p) Level

	Charge (C ₁)	Charge (C ₂)
	-0.239	-0.148
	-0.217	-0.058
	-0.264	0.039
	-0.232	0.055

Kinetically, the formation of $C_2Cl_3O + NO$ should be more favored than that of $C_2H_3O + NO$ for these two similar reactions.

Besides the dominant channel of $C_2Cl_3O + NO$, the reaction paths leading to several other product channels, i.e., $CCl_3CO + NO$, $CICNO + Cl_2CO$, and $Cl_2CCO + ClNO$, are also calculated to be accessible, and thus multiple reaction products CO , NO , Cl_2CO , and NO_2 corresponding to these channels are observed in the IR emission spectra. But for the $C_2H_3 + NO_2$ reaction, Geppert et al.'s calculation¹⁰ showed that the $C_2H_3O + NO$ channel seems to be the only energetically accessible reaction pathway. Another possible channel producing $C_2H_2 + HNO_2$ proceeds through the elimination of HNO_2 from the nitrite adduct C_2H_3ONO by surmounting a huge barrier which is $401.3 \text{ kJ}\cdot\text{mol}^{-1}$ above the reactants and thus is not accessible. In fact, only the product of NO was observed in their experiment. Other potential products including CH_3CO , $C_2H_3NO_2$, C_2H_2 , HNO_2 , and C_2H_3O were searched but not detected. In comparison to the $C_2H_3 + NO_2$ reaction, the chemical transformations of the $C_2Cl_3 + NO_2$ reaction are rich and complex.

In the initially formed adducts for the reaction of $C_2Cl_3 + NO_2$, both of the N-attack nitro adduct $C_2Cl_3-NO_2$ and O-attack nitrite adduct C_2Cl_3-ONO can be formed directly from the reactants and the O-attack addition is slightly more favorable in view of the binding energy. In comparison, for the reaction of $C_2H_3 + NO_2$, only the N-attack addition forming nitroethylene $C_2H_3-NO_2$ from the reactants was found to be plausible according to Geppert et al.'s calculation.¹⁰ Their calculations excluded the possibility of the O-attack addition forming vinyl nitrite C_2H_3-ONO from the reactants because the calculation of the formative process of the vinyl nitrite C_2H_3-ONO at different fixed C–O distances and all other geometry parameters variable showed that the nitrite geometry rearranges to the nitro geometry during this process.

For these two reactions of $C_2Cl_3 + NO_2$ and $C_2H_3 + NO_2$, the initial addition differs in the N-attack or O-attack association. This addition selectivity can be fundamentally correlated to the varied atomic charge of the radical site as a result of the chlorine substitution. Although this charge is not easily measurable, it can be consistently defined as, for example, in the Mulliken scheme in which an overlap charge density is divided equally between two atoms. These charges are calculated by Gaussian programs, and Table 2 shows the Mulliken atomic charge calculated at the level of B3LYP/6-311g(d,p). As the H atom

is substituted by Cl atom successively from C_2H_3 , C_2H_2Cl , C_2HCl_2 , to C_2Cl_3 the charge of the radical site C atom changes its polarity from negative to positive due to the electron-withdrawing induced effect of the Cl atom. Consequently, the addition of the reactant NO_2 (with the N atom positively charged by 0.332 and the O atom negatively charged by -0.166) to the radical C_2H_3 or C_2Cl_3 might be selectively different. The addition of NO_2 to C_2H_3 might be favored in the way of N-attack with the positively charged N atom being attached to the negatively charged C atom of the radical site, but the addition of NO_2 to C_2Cl_3 might be favored in the way of O-attack with the negatively charged O atom being attached to the positively charged C atom of the radical site. On the other hand, because both of the radical site C atom of the C_2Cl_3 (or C_2H_3) and the N-terminate of NO_2 have a single electron, the N-attack addition is expected to be plausible for both of the $C_2H_3 + NO_2$ and $C_2Cl_3 + NO_2$ reactions which can be regarded as recombination processes between two radicals.

Moreover, the chlorination affects the reaction thermochemistry. In view of the binding energies, the nitrite adduct C_2Cl_3-ONO ($284.9 \text{ kJ}\cdot\text{mol}^{-1}$ for the cis conformation) is more stable than the nitro adduct $C_2Cl_3-NO_2$ ($235.3 \text{ kJ}\cdot\text{mol}^{-1}$) for the $C_2Cl_3 + NO_2$ reaction, but on the contrary for the $C_2H_3 + NO_2$ reaction, i.e., the nitro adduct, $C_2H_3-NO_2$ ($313.6 \text{ kJ}\cdot\text{mol}^{-1}$) is more stabilized than the nitrite adduct C_2H_3-ONO ($301.9 \text{ kJ}\cdot\text{mol}^{-1}$ for the cis conformation).¹⁰ The decomposition of the nitrite adduct C_2Cl_3-ONO forming $C_2Cl_3O + NO$ (slightly exothermic by $2.4 \text{ kJ}\cdot\text{mol}^{-1}$) is more facile than the decomposition of the adduct C_2H_3-ONO forming $C_2H_3O + NO$ which requires $97.7 \text{ kJ}\cdot\text{mol}^{-1}$ of energy to break the O–N bond.¹⁰ Also, it is interesting to note that the exothermicity of a few channels in the $C_2H_3 + NO_2$ reaction is greatly reduced in the $C_2Cl_3 + NO_2$ reaction. For example, the $ClNO_2 + C_2Cl_2$ channel is only slightly exothermic by $0.8 \text{ kJ}\cdot\text{mol}^{-1}$, in comparison with the exothermicity of $203.8 \text{ kJ}\cdot\text{mol}^{-1}$ ¹⁰ for the analogous $HNO_2 + C_2H_2$ channel.

4. Conclusion

In summary, the products and mechanisms of the $C_2Cl_3 + NO_2$ reaction are investigated comprehensively by step-scan TR-FTIR spectroscopy and the CCSD(T)/6-311+G(d)//B3LYP/6-311G(d) level of electronic structure calculations. The $C_2Cl_3 + NO_2$ reaction exhibits rich and complex chemical transformations. The reaction proceeds through the isomerization and decomposition of the initially formed nitro ($C_2Cl_3-NO_2$) and nitrite (C_2Cl_3-ONO) adducts. There are mainly four energetically accessible reaction routes, i.e., the decomposition of the nitrite adduct forming $C_2Cl_3O + NO$ and its sequential dissociation to $CO + NO + CCl_3$, the elimination of $ClNO$ from the nitrite adduct leading to $ClNO + Cl_2CCO$, the Cl-atom shift of the nitrite adduct followed by the decomposition to $CCl_3CO + NO$, and the O-atom shift of the nitro adduct followed by the C–C bond cleavage forming $CICNO + Cl_2CO$. In competition with these reactive fluxes, the back-decomposition of the nitro or nitrite adducts leads to the prompt formation of vibrationally excited NO_2 , and the long-lived reaction adducts facilitate the vibrational energy transfer. Corresponding reaction products of CO , NO , Cl_2CO , and NO_2 are therefore observed in the time-resolved IR emission spectra.

In comparison to its analogous reaction $C_2H_3 + NO_2$, the mechanisms of the $C_2Cl_3 + NO_2$ reaction are similar and the dominant product channel is also the same, i.e., the decomposition of the nitrite adduct C_2Cl_3-ONO forming $C_2Cl_3O + NO$. Some differences do exist indicating that the chlorine substitu-

tion affects the reaction in the aspects of the reaction channels, thermochemistry, and reaction mechanisms. It is found that the two reactions mainly differ in the initial addition preferentially by the N-attack forming nitro adducts or the O-attack forming nitrite adducts. For the initial addition reaction of $C_2Cl_3 + NO_2$, both of the N-attack nitro adduct $C_2Cl_3-NO_2$ and O-attack nitrite adduct C_2Cl_3-ONO can be formed directly from the reactants and the O-attack addition is slightly more favorable in view of the binding energy. In comparison, for the initial addition reaction of $C_2H_3 + NO_2$, only the N-attack addition forming nitroethylene $C_2H_3-NO_2$ is plausible. On the basis of the Mulliken atomic charge calculation, this addition selectivity can be correlated to the variation of the charge density of the double-bond carbon atoms induced by the chlorine substitution due to the electron-withdrawing effect of chlorine groups.

Acknowledgment. This work is financially supported by the National Natural Science Foundation of China (Grant Nos. 20733005 and 20673126), the National Basic Research Program of China (2007CB815200, 2007AA02Z116), and the Chinese Academy of Sciences. Authors K.L. and T.X. contributed equally to this work.

References and Notes

- Zhao, Y.; Houk, K. N.; Olson, L. P. *J. Phys. Chem. A* **2004**, *108*, 5864.
- Ellison, G. B.; Herbert, J. M.; McCoy, A. B.; Stanton, J. F.; Szalay, P. G. *J. Phys. Chem. A* **2004**, *108*, 7639.
- Zhu, R. S.; Lin, M. C. *ChemPhysChem* **2004**, *5*, 1864.
- Bach, R. D.; Dmitrenko, O.; Estévez, C. M. *J. Am. Chem. Soc.* **2003**, *125*, 16204.
- Dixon, D. A.; Feller, D.; Zhan, C. G.; Francisco, J. S. *J. Phys. Chem. A* **2002**, *106*, 3191.
- Sayin, H.; McKee, M. L. *J. Phys. Chem. A* **2005**, *109*, 4736.
- Niki, H.; Maker, P. D.; Savage, C. M.; Breitenbach, L. P. *Chem. Phys. Lett.* **1978**, *59*, 78.
- Golden, D. M. *J. Phys. Chem. A* **2007**, *111*, 6772.
- Seeley, J. V.; Jayne, J. T.; Molina, M. J. *J. Phys. Chem.* **1996**, *100*, 4019.
- Geppert, W. D.; Eskola, A. J.; Timonen, R. S.; Halonen, L. *J. Phys. Chem. A* **2004**, *108*, 4232.
- Senkan, S. M.; Robinson, J. M.; Gupta, A. K. *Combust. Flame* **1983**, *49*, 305.
- Valeiras, H.; Gupta, A. K.; Senkan, S. M. *Combust. Sci. Technol.* **1984**, *36*, 123.
- Taylor, P. H.; Tirey, D. A.; Rubey, W. A.; Dellinger, B. *Combust. Sci. Technol.* **1994**, *101*, 75.
- Taylor, P. H.; Tirey, D. A.; Dellinger, B. *Combust. Flame* **1996**, *104*, 260.
- Russell, J. J.; Seetula, J. A.; Gutman, D.; Senkan, S. M. *J. Phys. Chem.* **1989**, *93*, 1935.
- Kostina, S. A.; Bryukov, M. G.; Shestov, A. A.; Knyazev, V. D. *J. Phys. Chem. A* **2003**, *107*, 1776.
- Wang, H.; Li, J.; Song, X.; Li, Y.; Hou, H.; Wang, B.; Su, H.; Kong, F. *J. Phys. Chem. A* **2006**, *110*, 10336.
- Xiang, T.; Liu, K.; Zhao, S.; Su, H.; Kong, F.; Wang, B. *J. Phys. Chem. A* **2007**, *111*, 9606.
- Xiang, T.; Liu, K.; Su, H. *Chin. J. Chem. Phys.* **2007**, *20*, 407.
- Seakins, P. W. *The Chemical Dynamics and Kinetics of Small Radicals*; Liu, K., Wagner, A., Eds.; World Scientific: Singapore, 1995; pp 250–314.
- Becke, A. D. *J. Chem. Phys.* **1993**, *98*, 5648.
- Lee, C.; Yang, W.; Parr, R. G. *Phys. Rev. B* **1988**, *37*, 785.
- Gonzalez, C.; Schlegel, H. B. *J. Phys. Chem.* **1989**, *90*, 2154.
- Frisch, M. J.; Trucks, G. W.; Schlegel, H. B.; Scuseria, G. E.; Robb, M. A.; Cheeseman, J. R.; Montgomery, J. A., Jr.; Vreven, T.; Kudin, K. N.; Burant, J. C.; Millam, J. M.; Iyengar, S. S.; Tomasi, J.; Barone, V.; Mennucci, B.; Cossi, M.; Scalmani, G.; Rega, N.; Petersson, G. A.; Nakatsuji, H.; Hada, M.; Ehara, M.; Toyota, K.; Fukuda, R.; Hasegawa, J.; Ishida, M.; Nakajima, T.; Honda, Y.; Kitao, O.; Nakai, H.; Klene, M.; Li, X.; Knox, J. E.; Hratchian, H. P.; Cross, J. B.; Bakken, V.; Adamo, C.; Jaramillo, J.; Gomperts, R.; Stratmann, R. E.; Yazyev, O.; Austin, A. J.; Cammi, R.; Pomelli, C.; Ochterski, J. W.; Ayala, P. Y.; Morokuma, K.; Voth, G. A.; Salvador, P.; Dannenberg, J. J.; Zakrzewski, V. G.; Dapprich, S.; Daniels, A. D.; Strain, M. C.; Farkas, O.; Malick, D. K.; Rabuck, A. D.; Raghavachari, K.; Foresman, J. B.; Ortiz, J. V.; Cui, Q.; Baboul, A. G.; Clifford, S.; Cioslowski, J.; Stefanov, B. B.; Liu, G.; Liashenko, A.; Piskorz, P.; Komaromi, I.; Martin, R. L.; Fox, D. J.; Keith, T.; Al-Laham, M. A.; Peng, C. Y.; Nanayakkara, A.; Challacombe, M.; Gill, P. M. W.; Johnson, B.; Chen, W.; Wong, M. W.; Gonzalez, C.; Pople, J. A. *Gaussian 03*, revision B03; Gaussian Inc.: Pittsburgh, PA, 2003.
- NIST Chemical Kinetics Database; <http://kinetics.nist.gov/StandardReferenceDatabase17-2Q98>; National Institute of Standards and Technology: Gaithersburg, MD.
- Berry, M. J. *J. Chem. Phys.* **1974**, *61*, 3114.
- Umemoto, M.; Seki, K.; Shinohara, H.; Nagashima, U.; Kinoshita, M.; Shimada, R. *J. Chem. Phys.* **1985**, *83*, 1657.
- Suzuki, T.; Tonokura, K.; Bontuyan, L. S.; Hashimoto, M. *J. Phys. Chem.* **1994**, *98*, 13447.
- Tonokura, K.; Daniels, L. B.; Suzuki, T. *J. Phys. Chem. A* **1997**, *101*, 7754.
- Sato, K.; Tsunashima, S.; Takayanagi, T.; Fujisawa, G.; Yokoyama, A. *J. Chem. Phys.* **1997**, *106*, 10123.
- Blank, D. A.; Sun, W.; Suits, A. G.; Lee, Y. T.; North, S. W.; Hall, G. E. *J. Chem. Phys.* **1998**, *108*, 5414.
- Lee, Y. J.; Lee, Y. R.; Chou, C. C.; Lin, S. M. *J. Chem. Phys.* **1998**, *109*, 346.
- Su, H.; Yang, J.; Ding, Y.; Feng, W.; Kong, F. *Chem. Phys. Lett.* **2000**, *326*, 73.
- Zou, P.; Klippenstein, S. J.; Osborn, D. L. *J. Phys. Chem. A* **2005**, *109*, 4921.